Overview of microfabricated bolometers with vertically aligned carbon nanotube absorbers

Cite as: AIP Advances **10**, 055010 (2020); https://doi.org/10.1063/5.0004025
Submitted: 07 February 2020 • Accepted: 22 April 2020 • Published Online: 07 May 2020

N. A. Tomlin, C. S. Yung, Z. Castleman, et al.

Overview of microfabricated bolometers with vertically aligned carbon nanotube absorbers

Cite as: AIP Advances 10, 055010 (2020); doi: 10.1063/5.0004025
Submitted: 7 February 2020 • Accepted: 22 April 2020 •
Published Online: 7 May 2020

N. A. Tomlin,[1,a)] C. S. Yung,[1] Z. Castleman,[2] M. Denoual,[3] G. Drake,[2] N. Farber,[2] D. Harber,[2] K. Heuerman,[2] G. Kopp,[2] H. Passe,[2] E. Richard,[2] J. Rutkowski,[2] J. Sprunck,[2] M. Stephens,[1] C. Straatsma,[2] S. Van Dreser,[2] I. Vayshenker,[1] M. G. White,[1,4] S. I. Woods,[5] W. Zheng,[2] and J. H. Lehman[1]

AFFILIATIONS

[1]National Institute of Standards and Technology (NIST), Boulder, Colorado 80305, USA
[2]Laboratory for Atmospheric and Space Physics (LASP), Boulder, Colorado 80303, USA
[3]GREYC-electronique, ENSICAEN, University of Caen Basse-Normandie, 14000 Caen, France
[4]Department of Physics, University of Colorado, Boulder, Colorado 80309, USA
[5]National Institute of Standards and Technology (NIST), Gaithersburg, Maryland 20899, USA

[a)]**Author to whom correspondence should be addressed:** nathan.tomlin@nist.gov

ABSTRACT

Multi-wall vertically aligned carbon nanotubes (VACNTs) are nearly ideal absorbers due to their exceptionally low reflectance over a broad wavelength range. Integrating VACNTs as bolometer absorbers, however, can be difficult due to their high growth temperature and fragile nature. Despite these challenges, we have microfabricated many different types of VACNT bolometers, ranging from cryogenic optical power primary standards to room temperature satellite-based solar irradiance monitors and broadband infrared microbolometers. Advantages our VACNT bolometers provide over the bolometers they replace vary by application, but can be reduced size and time constant, increased absorption, and/or microfabrication instead of hand assembly. Depending on the application and operating conditions, our VACNT bolometers are designed with a variety of thermistors and weak thermal links. The thermistors used include commercial surface mount chips, superconducting transition-edge sensors, and vanadium oxide (VO_x). Weak thermal links include silicon nitride (SiN_x) membranes, Si bridges, and laser-cut polyimide. We summarize a wide variety of microfabricated bolometers with VACNT absorbers that measure optical power levels spanning over seven orders of magnitude.

I. INTRODUCTION

Bolometers are desirable for applications requiring SI traceability, broadband detection, and/or absorption in the near infrared or at longer wavelengths. Multi-wall vertically aligned carbon nanotubes (VACNTs) (Fig. 1) are excellent absorbers having high absorptance over a broad wavelength range (can absorb >99% of light from 0.3 μm to 50 μm).[1–4] Unfortunately, incorporation of VACNT absorbers with microfabricated bolometers can be problematic. The high temperature required for VACNT growth (typically >600 °C) limits the materials and fabrication steps that can be performed before VACNT growth. Additionally, the fragile nature of the high aspect ratio VACNTs severely limits the fabrication steps that can be performed after VACNT growth (i.e., no physical touch or solvents).

Below, we discuss the solutions we have found to overcome these limitations to build a wide variety of microfabricated VACNT bolometers that work at temperatures from 4 K to 320 K, in space and in the lab, and with time constants from 30 ms to 400 s.

II. FABRICATION

In addition to an absorber, a bolometer also requires a substrate, a weak thermal link, thermistor(s), and electrical wiring. In

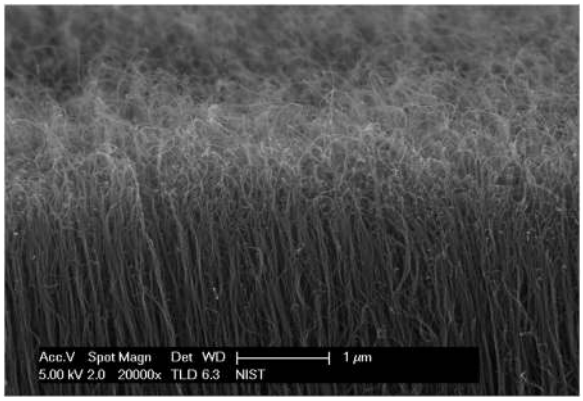

FIG. 1. Scanning electron microscope (SEM) image of VACNTs.

order to achieve absolute accuracy and closed loop operation, an electrical heater is also needed for electrical substitution heating.[5] The method we typically use to fabricate bolometers with VACNTs is to only use materials and process steps that are compatible with high temperatures and grow VACNTs as the final fabrication step, which we call a high temperature last process (alternative process options are discussed in Appendix A).

The substrate for all our bolometers is silicon, and the first fabrication step is to grow a thermal SiO_2 layer on a silicon wafer at 1100 °C in a tube furnace. In order to remain electrically insulating after VACNT growth, a minimum thickness is required; a thickness of 150 nm of SiO_2 is often too thin and can develop shorts to the underlying silicon substrate, but a thickness of ≥500 nm remains insulating. For devices requiring membranes, we then deposit low stress silicon nitride (SiN_x) by low pressure chemical vapor deposition (LPCVD) at 835 °C in a separate tube furnace.

Thin film metal layers used for wiring, heaters, and some thermistors are typically deposited by magnetron sputtering and patterned by photoresist lift-off. Our metal of choice is W (melting point 3422 °C) for the electrical heater and room temperature wiring. In the past, we have used Mo (melting point 2623 °C), but after VACNT growth, the films tend to oxidize and gradually disappear with time, especially when exposed to water vapor. Many thin film metals with bulk melting temperatures significantly above VACNT growth temperatures are not compatible with VACNT growth. For example, films of Au, Ni, and Pt, with melting points of 1063 °C, 1453 °C, and 1768 °C, respectively, tend to disappear or form islands and are no longer electrically conducting after VACNT growth. Other metals can increase in resistivity after VACNT growth by a factor of 10 or more, unless an overlayer of SiO_2 or SiN_x is deposited by plasma-enhanced chemical vapor deposition (PECVD) or magnetron sputtering.

Thermistors can be grown, deposited, or attached, depending on the type of thermistor and application. Thermistors are discussed in detail in Sec. III.

We have not yet successfully developed an electrically insulating layer between two metal layers or between a metal layer and VACNTs that remains insulating after VACNT growth. PECVD of SiO_2 and SiN_x does not remain insulating for thin films (≤150 nm), and thicker films tend to blister and/or peel during the high temperature VACNT growth. Additionally, sputter-deposited thin films (≤100 nm) of aluminum oxide (AlO_x) or aluminum nitride (AlN) are also no longer insulating after VACNT growth. As a consequence, the high temperature last process flow is currently not compatible with electrical substitution heaters underneath the VACNT absorber. Instead, heaters must either surround the VACNT absorber or be placed on the opposite side of the Si substrate.

The VACNT growth area is controlled by patterning two sputter-deposited layers, a catalyst support layer of AlO_x or AlN 10–20 nm thick, followed by a catalyst layer of Fe 0.5–2 nm thick.

Typical weak thermal links used for bolometers are SiN_x membranes or Si beams formed by Bosch-process deep reactive ion etching (DRIE).[6]

After all other fabrication steps are finished, VACNTs are grown on individual bolometer chips in a cold-wall PECVD system, typically at 750 °C to 850 °C, while flowing Ar, H_2, and C_2H_4 at a total pressure of 2666.5 Pa (20 Torr), and an applied microwave power of 900 W. Growth times are typically 1–60 min, depending on the desired height of the VACNTs. The multi-wall VACNTs grown in our system exhibit base-growth, have diameters of 10–20 nm, and are vertically aligned due to neighbor crowding (Fig. 1).[7,8] We have measured a VACNT volumetric mass density of 40.5 kg m^{-3} and the volumetric heat capacity from 310 K to 2 K (see Fig. 12 and Appendix B for details). The VACNTs are robust to spraying with compressed gas, but cannot be physically touched or exposed to liquids.[9] However, it has been found that a different type of VACNT, aligned by an electric field, is more robust to liquids.[10]

Occasionally, separate metallic traces are found to be shorted together after VACNT growth, presumably due to deposition of amorphous carbon during the VACNT growth process. The electrical shorting can be removed by an oxygen plasma (ash) at an RF power of 50 W (30 kHz) at 66.67 Pa (0.5 Torr) for 20 s. Exposure to plasma at higher power and longer duration can reduce the VACNT reflectance (see Appendix C and Fig. 14), but we tend to avoid this because it changes the VACNTs from hydrophobic to hydrophilic.[3,11] Additionally, after VACNT growth, if the fabricated device is large enough, it is possible to attach commercial thermistors (see Sec. III D).

Process steps for all the bolometers discussed in this paper are listed in Appendix D.

III. THERMISTOR OPTIONS

Thermistors for each bolometer are chosen based on their performance, operating temperature, and compatibility with fabrication steps. A common figure of merit for thermistors is the temperature coefficient of resistance (TCR = $1/R \cdot dR/dT$), expressed in this paper as %/K, where R is the resistance, and T is the temperature. Table I contains a summary of each thermistor discussed.

A. VACNT thermistors

VACNTs have a temperature dependent resistance and are an option for use as cryogenic thermistors.[12–15] Typical TCRs are −25%/K below 5 K. While VACNT thermistors are desirable for simplicity, we have found them to have repeatability issues

TABLE I. Summary of thermistors known to be compatible with VACNT growth.

Thermistor	TCR (%/K)	Operating temperature (K)
VACNT	−25	≤10
Superconductor	500–2000	≤13
Metal	≤0.5	Any
Commercial	−4	250–350
VO_x	−1.2	250–350

(nominally identical thermistors can differ by orders of magnitude in resistance).

B. Superconducting thermistors

We have found that a surprising number of metals are superconducting after VACNT growth despite the Fe catalyst and high growth temperature. We performed a cursory exploration of the superconducting transition critical temperature (T_c) of some thin film metals with and without PECVD SiN_x overlayers (Fig. 2). The commercial refrigerator we used for the task had a base temperature of 4 K. Some of the variabilities in the data are due to differing growth temperatures (750 °C to 850 °C), differing growth times (15–60 min), and post-growth rapid thermal anneals in N_2 (just for Mo). Superconducting thin films used as thermistors by biasing in the transition are called transition-edge sensors (TESs).[16] While many of the superconducting transitions are broadened by VACNT growth, others remain narrow. For example, we typically measure post-VACNT growth Nb TCRs of 500%/K to 2000%/K. Bolometers utilizing TESs are discussed in Sec. IV.

C. Metal film thermistors

Any metal film can be used as a thermistor over a wide temperature range. However, the main drawback is poor sensitivity, as metals have positive TCRs that are typically less than 0.5%/K. Bolometers utilizing metal thermistors are discussed in Sec. V C.

D. Commercial thermistors

If a bolometer is large enough, it is possible to attach commercial thermistors after fabrication. Some advantages are that the thermistor does not have to survive high temperature VACNT growth, and commercial thermistors can have excellent performance with low intrinsic noise and high sensitivity (TCRs up to −4%/K at room temperature). Disadvantages are size and speed constraints because commercial thermistors are large compared to typical microfabrication dimensions, and hand assembly is time intensive and can be difficult to reproduce. For room temperature use, we have measured different types of commercial surface mount thermistors, mainly focusing on finding the lowest noise thermistors.[17,18] Initially, we used thermistors with contact pads on opposite faces, where the bottom pad was attached with an electrically conductive epoxy to a thin film metal pad, and the top pad was wirebonded to another thin film metal pad [Fig. 3(a)]. However, we found that the conductive epoxy joint was too variable and could be a large source of noise. We measure much more consistently low noise results using surface mount Semitec FT thermistors, which have both contact pads on the top surface. These thermistors are physically anchored to the bolometers with thermally conductive epoxy, and both electrical connections are made with wirebonds, avoiding having any conductive epoxy in the electrical circuit [Fig. 3(b)]. Bolometers utilizing commercial thermistors are discussed in Secs. V A, V B, and V D.

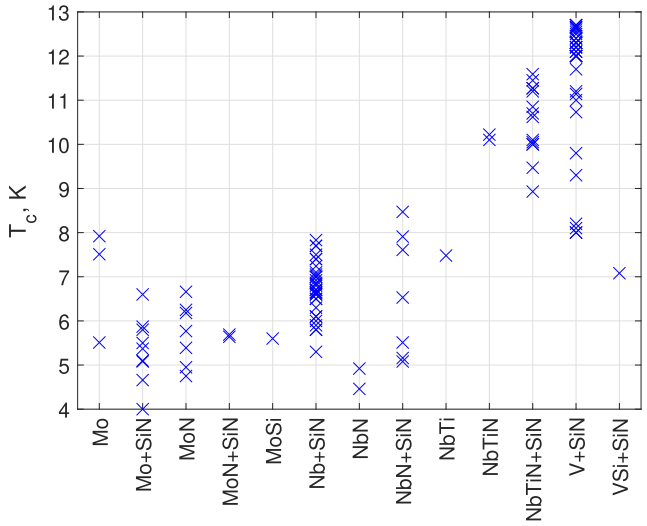

FIG. 2. Plot of superconducting transition critical temperature (T_c) for different superconducting thin films after VACNT growth. The thin film compositions are not stoichiometric, and subscripts have been omitted for clarity. Labels with "+SiN" signify that a PECVD overlayer of SiN_x has been deposited over the metal.

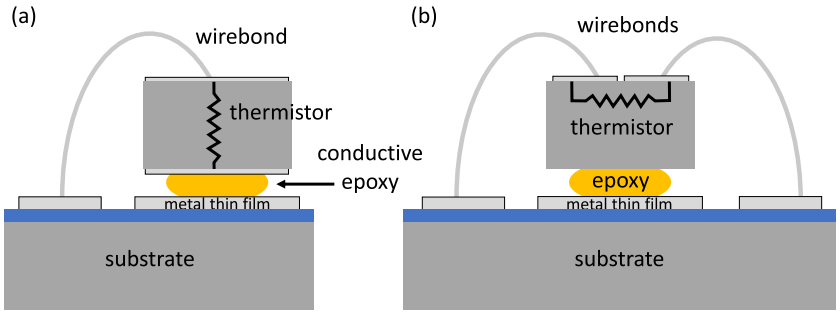

FIG. 3. Side view schematics of two commercial thermistor attachment approaches. Electrically conductive epoxy is part of the electrical circuit in (a), but not in (b).

E. Vanadium oxide thermistors

For room temperature bolometers that are small or where speed is important, we have developed vanadium oxide (VO_x) thin film thermistors that are compatible with VACNT growth.[4] While commercial, optimized VO_x thermistors can have TCRs of −4%/K, our initial results have achieved TCRs close to −3%/K for as-sputtered VO_x films and −1.2%/K for post-VACNT growth VO_x films. Bolometers utilizing VO_x thermistors are discussed in Sec. V E.

IV. CRYOGENIC BOLOMETERS

Cryogenic bolometers are used by national metrology institutes around the world for the most accurate and precise measurements of optical power. Operation at cryogenic temperatures has many benefits, including reduced radiative coupling, increased thermal conductivity, reduced heat capacity, and superconducting wiring. The absorbers in these systems are typically conical or cylindrical cavities coated with specular black paint and designed so that incoming light undergoes multiple reflections, absorbing ≥99.95% of incident light (≤500 ppm reflected).

Planar VACNTs can absorb light nearly as well as traditional cryogenic bolometer cavities with only a single light–surface interaction (Fig. 14).[3] A planar absorber allows for cryogenic bolometers with greatly reduced size and time constant, and allows for microfabrication instead of hand assembly. The planar cryogenic radiometer (PCR) operates below 7 K and has a narrow Si beam weak thermal link, a Nb TES thermistor with a T_c near 7 K, a W electrical heater, and V with a SiN_x overlayer for the superconducting wiring with a T_c near 12 K [Figs. 4(a) and 4(b)].[15,19,20] The PCR can measure wavelengths from 458 nm to 1550 nm (limited by available laser sources and reflectance measurements), and input power levels from 10 μW to 1 mW, with an uncertainty (k = 2) of 0.02% (200 ppm).[19] A fiber-coupled setup, called the fiber-coupled cryogenic radiometer (FCCR), is used to measure optical fiber power at wavelengths of 850 nm, 1295 nm, and 1550 nm, and input power levels from 10 μW to 1 mW, with an uncertainty (k = 2) of 0.1% (1000 ppm) [Fig. 4(c)].[21]

At cryogenic temperatures, VACNTs contribute significantly to the total heat capacity of the bolometer (see Fig. 12). Therefore, we reduced the size of the PCR absorber [Fig. 4(b)] to make it faster (time constant ≤20 ms) for use with a Fourier-transform infrared (FTIR) spectrometer being developed at the NIST low background infrared (LBIR) facility.[22]

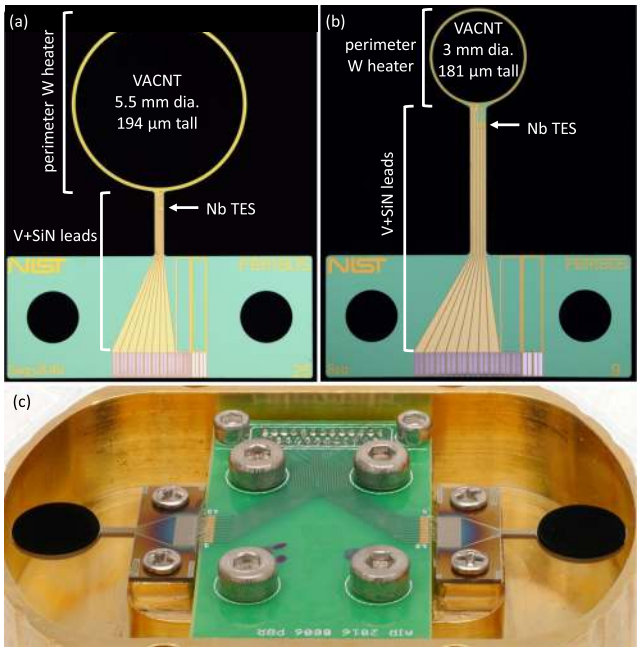

FIG. 4. [(a) and (b)] Images of two planar cryogenic radiometers (PCRs) (each image is a photo-stitched combination of two microscope images). In (b), the size of the absorber has been reduced to decrease the time constant. (c) Multiple images digitally combined (focus-stacked) of two PCRs in the fiber-coupled cryogenic radiometer (FCCR) (optical fibers not shown).

V. ROOM TEMPERATURE BOLOMETERS

Compared to cryogenic bolometers, operating bolometers near room temperature allows them to be much simpler, cheaper, and smaller. This in turn leads to applications that are more numerous and varied. However, room temperature bolometers have to contend with radiative coupling and resistive wiring, which typically leads to larger uncertainties in measurements.

A. Satellite-based solar spectral irradiance

The compact spectral irradiance monitor (CSIM) is a 6U (1U = 10 × 10 × 11.35 cm^3) CubeSat that was successfully launched on December 3, 2018.[23] Solar spectral irradiance is monitored by three photodiodes, with VACNT bolometers providing traceability. The CSIM has two identical channels, and each channel has a bolometer. The two bolometers are operated in an AC resistance bridge in order to cancel common-mode temperature drifts. Each bolometer has a 2 μm thick SiN_x membrane weak thermal link, a commercial thermistor, and W electrical heater and wiring (Fig. 5). The open-loop time constant is 25 s, and the closed-loop time constant is <1 s. The entrance slit into the instrument is 165 μm by 5 mm. The bolometers measure wavelengths from 200 nm to 2800 nm, and input power (irradiance) from 10 nW (12.1 mW m^{-2}) to 40 μW (48.5 W m^{-2}), with a noise floor below 0.5 nW (606 μW m^{-2}).

Mainly due to a compact optical design, the CSIM is smaller and lower-cost than the current spectral irradiance monitor (SIM) on the total and spectral solar irradiance sensor (TSIS-1) operating from the International Space Station. The electrical substitution bolometers on the TSIS-1 SIM have etched nickel phosphorous (NiP) black absorbers and are entirely hand assembled over 14 months. Compared to the TSIS-1 SIM bolometers, the CSIM VACNT bolometers are similar in size, but have 7.2 times lower noise, and the microfabrication is much faster (2 weeks) and more reproducible.

B. Satellite-based solar total irradiance

The compact total irradiance monitor (CTIM), currently being developed, is a 6U CubeSat with eight VACNT bolometers,

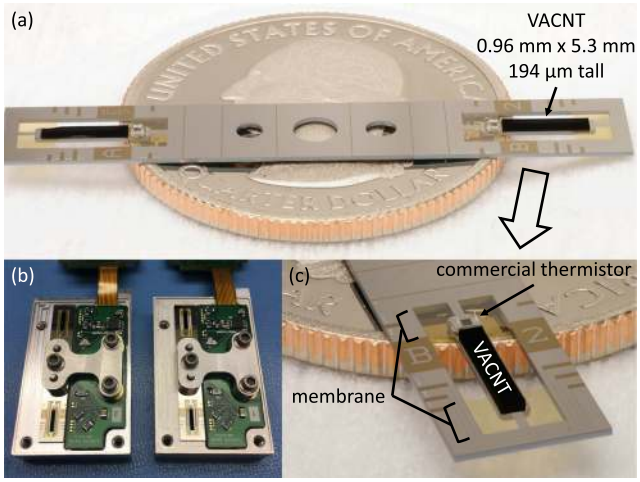

FIG. 5. [(a) and (c)] Focus-stacked images of compact spectral irradiance monitor (CSIM) bolometers shown on a US quarter for scale. The heater is a W meander outside the long edges of the VACNTs, but is not visible without further magnification. (b) Image of two CSIM bolometer chips with readout electronics.

scheduled for launch in 2021.[24] Each CTIM bolometer has a weak thermal link of three laser-cut polyimide legs, four commercial thermistors wired in parallel, and W electrical heater and wiring [Fig. 6(a)]. A reflecting dome of 51 μm thick Cu plated with Au is epoxied to each bolometer, further reducing the reflectance of the VACNTs by a factor of 10 [Fig. 6(b)]. The bolometers are operated in pairs in an AC resistance bridge. The open-loop time constant is >400 s and the closed-loop time constant is <2 s. The CTIM bolometers measure the full solar spectrum (100 nm to 50 μm) through a 5 mm diameter aperture at an input power (irradiance) of 26.7 mW (1361 W m^{-2}) and a noise floor below 30 nW (1.5 mW m^{-2}).

With a compact and simplified design, CTIM will be smaller and lower cost than the current total irradiance monitor (TIM) on TSIS-1. The electrical substitution bolometers on TSIS-1 TIM have conical cavities coated with etched NiP black and take approximately 12 months to hand assemble with a yield of ≈15%. Compared to the TSIS-1 TIM bolometers, the CTIM VACNT bolometers are much smaller (planar instead of cavities) and are microfabricated much faster (2 weeks) with a higher yield (≈80%).

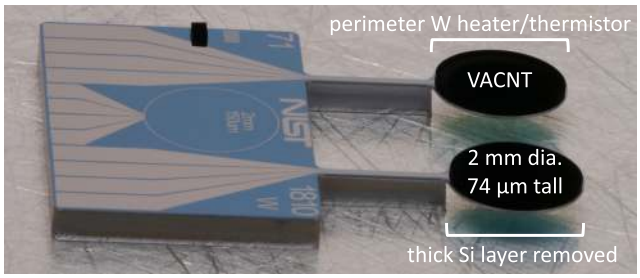

FIG. 7. Focus-stacked image of a bolometer for a potential pyranometer.

C. Ground-based solar irradiance

A pyranometer is being developed with the company Kipp and Zonen based in the Netherlands.[25] The pyranometer bolometer has a narrow Si beam weak thermal link, a W perimeter trace that functions as both thermistor and heater, and W wiring (Fig. 7). The bolometer is fabricated on a silicon-on-insulator (SOI) wafer, so that the Si under the VACNT absorber can be thinned to decrease the time constant of the device below 100 ms. Two identical bolometers are operated together in order to cancel common-mode temperature drifts. The goal is to measure irradiances up to 1500 W m^{-2} with a resolution below 1 W m^{-2}.

Current commercial pyranometers have planar diffuse black paint absorbers that are typically <99% absorbing. A VACNT-based pyranometer would have higher absorption, and the spectral response would be flatter across the solar spectrum.

D. Laser power metrology

We have developed a VACNT bolometer for laser power metrology with a narrow Si beam for a weak thermal link, two commercial thermistors per bolometer, and W electrical heater and wiring (Fig. 8). The bolometer is designed to measure laser powers from 100 μW to 300 mW with an uncertainty of 0.3% and wavelengths from 244 nm to 1930 nm.[26] The open-loop time constant is 23 s. The next version of this bolometer, currently in development, will be more similar to the CTIM (see Sec. V B), but modified for higher power, lower inequivalence, and lower uncertainty.[27]

The VACNT bolometer replaces the 50 year old NIST calorimeter (C-Series), which has an absorber cavity coated in black paint.[28] Compared to the C-Series, the main advantage of the VACNT

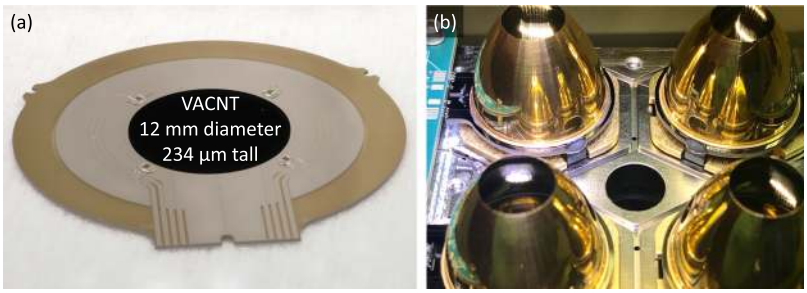

FIG. 6. (a) Focus-stacked image of a compact total irradiance monitor (CTIM) bolometer without a dome. (b) Image of four CTIM bolometers. Epoxy can be seen on three of the polyimide legs, but more recent devices do not use epoxy.

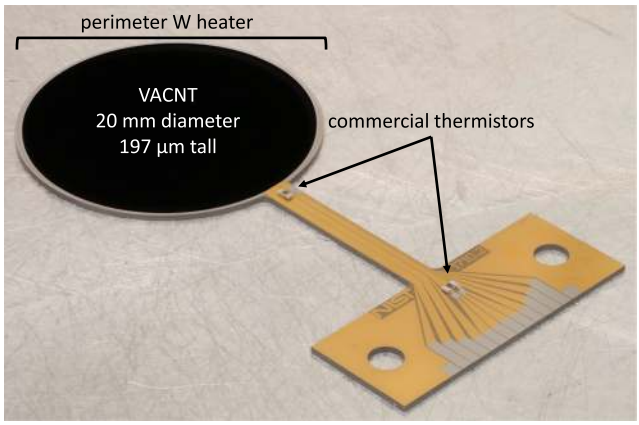

FIG. 8. Focus-stacked image of a bolometer for laser power metrology.

bolometer is a reduction in time constant of more than an order of magnitude.

E. Microbolometers

We are currently developing VACNT microbolometer linear arrays, where the bolometer weak thermal link is 2–4 SiN_x legs, a VO_x thin film functions as both the thermistor and heater, and the wiring is W (Fig. 9).[4] Depending on the membrane size and thermal

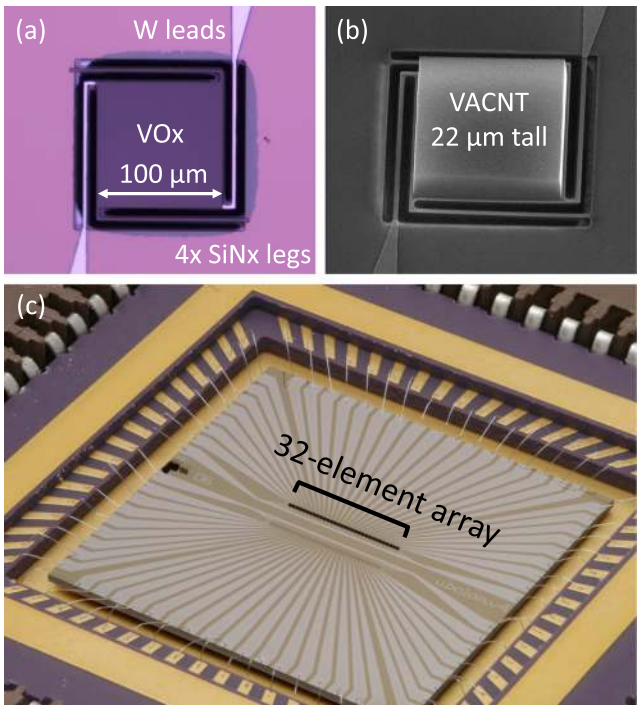

FIG. 9. (a) Microscope image of a single microbolometer pixel before VACNT growth. (b) SEM image of a single microbolometer pixel. (c) Focus-stacked image of a 32-element microbolometer linear array.

TABLE II. Summary of the bolometers discussed in Secs. IV and V. For devices that measure irradiance, stated irradiance values have been converted to power.

Bolometer	Power range	Expanded uncertainty (ppm)	Operating temperature (K)
PCR	10 μW–1 mW	200	<7
FCCR	10 μW–1 mW	1000	<7
CSIM	10 nW–40 μW	10 000	≈300
CTIM	26.7 mW	194	≈300
Pyranometer	6 mW	1,333[a]	≈300
Laser metrology	100 μW–300 mW	3000	≈300
Microbolometers	50 nW	40 000[a]	≈300

[a]Estimated uncertainty, not yet measured.

link design, open-loop time constants are typically 30–60 ms, and closed-loop time constants are 10–20 ms. For an Earth radiance of 90 W m^{-2} sr^{-1}, a 500 km orbit, a 15 mm aperture, and a 1 km ground pixel size, each pixel will receive an incident power of 50 nW. Initial results show a noise level of 1 nW at 10 Hz; however, we are working to optimize the microbolometers and lower the noise.

Currently, Earth's outgoing longwave radiation (OLW) from 3 μm to 100 μm is measured by Clouds and the Earth's Radiant Energy System (CERES) satellites. Each CERES satellite has three identical bolometers with filters to measure different wavelength bands. Each bolometer consists of two thermistor flakes, coated with black paint and operated in a bridge readout.[29] In order to get spatial resolution from a single element, the instrument must be scanned, which makes it large and expensive. Size and cost could be reduced by using microbolometer linear arrays without scanning, but commercial far-IR arrays are narrowband and limited to wavelengths of 7–15

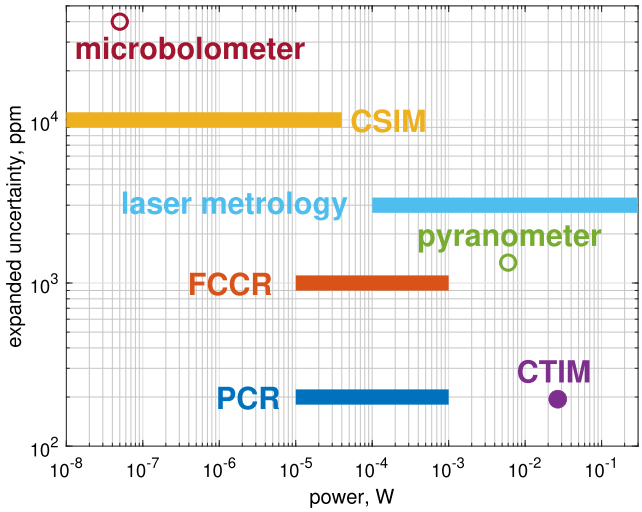

FIG. 10. Plot of expanded uncertainty (k = 2) vs input power for the completed bolometers discussed in Secs. IV and V. For devices that measure irradiance, stated irradiance values have been converted to power. An open circle indicates the estimated uncertainty.

μm. Exceptions are recently modified commercial microbolometer arrays with gold black absorbers to make them broadband.[30,31]

VI. SUMMARY AND CONCLUSIONS

While VACNT absorbers have many benefits for bolometers, their use has been limited by fabrication challenges due to high temperature growth and fragility. We have overcome these challenges to microfabricate a wide range of VACNT bolometers. Applications such as cryogenic radiometry, solar irradiance monitoring, and laser power metrology benefit from VACNT absorbers because they have high absorptance and are planar and compatible with microfabrication, which allows for smaller, faster, cheaper, and more reproducible bolometers. Excellent broadband absorption out to tens of micrometers will enable future SmallSat microbolometer arrays for monitoring Earth's outgoing longwave radiation. The performance of the VACNT bolometers discussed above is summarized in Table II and Fig. 10, showing a span in measured power of over seven orders of magnitude.

ACKNOWLEDGMENTS

Funding for CSIM, CTIM, and microbolometer development was provided by the National Aeronautics and Space Administration (NASA) Earth Science Technology Office (ESTO). Trade names are identified only for reference purposes and do not imply recommendation or endorsement by the NIST.

APPENDIX A: ALTERNATIVE FABRICATION PROCESSES

The high temperature last process discussed in Sec. II is just one fabrication process that is known to work for VACNT bolometers. Below, we discuss three additional process options that could potentially be used.

1. High temperature first process

A novel method of fabricating VACNT bolometers is to first grow the VACNTs in recessed wells on Si or a SiN_x membrane, which can then be protected by a cover during subsequent fabrication steps (Fig. 11).[32] The cover can be another wafer electrostatically bonded or attached with epoxy. The VACNTs are then protected from physical contact from subsequent processing steps, and the subsequent layers do not need to survive the high temperature VACNT growth. After the device is fabricated, the protective cover can be removed or left in place. If the VACNTs are grown on a SiN_x membrane, one difficulty is that the membranes have to be strong enough to survive fabrication steps and have to remain solid (no vias or legs). However, in order to weaken the thermal link, a focused ion beam (FIB) could be used to mill holes in finished membranes.[33,34]

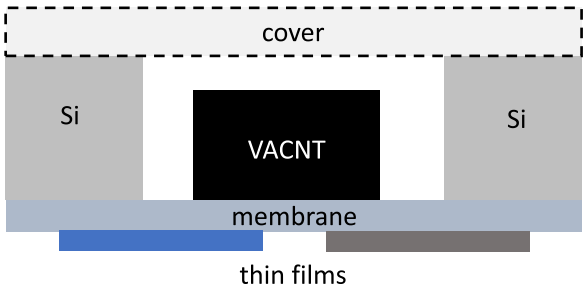

FIG. 11. Cross-section schematic of a high temperature first process, where VACNTs are recessed and covered.

2. No high temperature process

An option to separate the VACNT high temperature processing from the bolometer fabrication is to grow the VACNTs on a separate wafer and transfer them to a finished bolometer. When VACNTs are exposed to a dilute HF acid solution, the VACNTs can float off the growth substrate and can then be transferred to a new substrate.[35–37] A dry transfer following a weak oxidation is another option.[38] With either transfer method, placement of the VACNTs is much less precise than defining them lithographically, but if necessary, VACNTs can then be removed from unwanted areas using a laser.[30]

3. Localized high temperature process

A final process option for integrating VACNTs is to limit heating to local areas, where VACNT growth is desired, which has been shown to work using on-chip heaters and laser heating.[39–44]

APPENDIX B: VACNT DENSITY AND HEAT CAPACITY

In order to measure the VACNT mass and density, we prepared square Si chips 2 mm on a side and grew VACNTs on some of the samples. The samples with and without VACNTs were weighed using a commercial microbalance with a readability of 0.1 μg. For 250 μm tall VACNTs, we measure a volumetric mass density of 40.5 kg m^{-3}. Assuming that the individual carbon nanotubes have a volumetric mass density of graphite (2160 kg m^{-3}), this gives a VACNT fill factor of 1.9%.

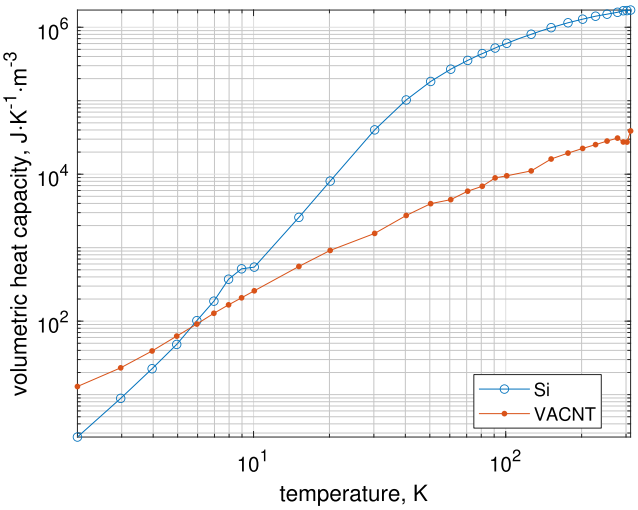

FIG. 12. Measured volumetric heat capacity of Si and VACNTs vs temperature.

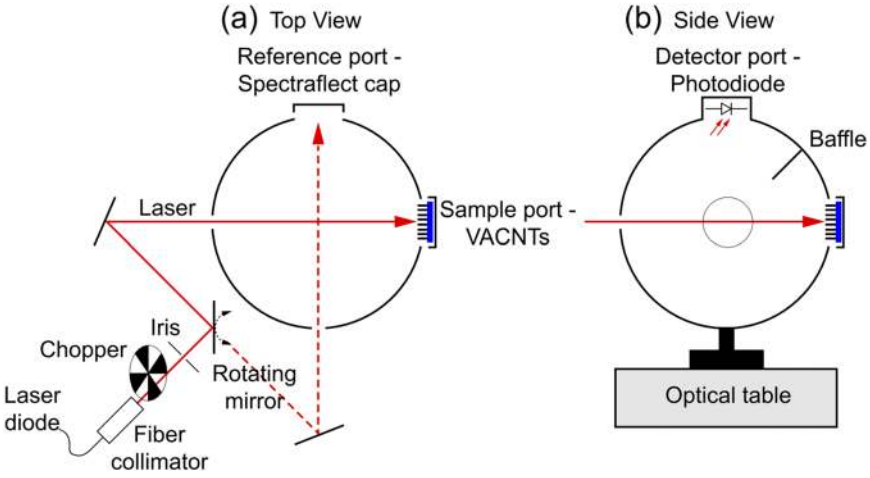

FIG. 13. Reprinted with permission from Yung *et al.*, Carbon **127**, 195–201 (2018). Copyright 2018 Elsevier. (a) Top view cross section of the $d = 0°/h$ measurement. The solid red line depicts the laser beam path for the sample measurement, and the dotted red line depicts the path for the reference measurement. (b) Side view cross section of the measurement.

We measured the VACNT heat capacity using a commercial heat capacity system, consisting of a small microcalorimeter platform (3 mm on a side) with a thermistor and heater, suspended by eight wires. A small amount of cryogenic grease was applied to the platform, and the heat capacity was measured from 310 K to 2 K. A sample with VACNTs on a square Si chip 2 mm on a side was then attached to the platform, and the heat capacity was measured again. Finally, the VACNTs were scraped off the Si, and the heat capacity was measured a third time. The three separate measurements allow the Si and VACNT volumetric heat capacities to be extracted, as shown in Fig. 12.

APPENDIX C: DIRECTIONAL-HEMISPHERICAL REFLECTANCE (d/h)

The directional-hemispherical reflectance at normal incidence ($d = 0°/h$) was measured using a 152.4 mm (6 in.) diameter integrating sphere with a Spectraflect coating (97% diffuse reflectance).[3] Eleven thermoelectrically cooled fiber-coupled laser diodes were used as sources, ranging in wavelength from 220 nm to 1650 nm. Samples were square Si chips 17 mm on a side, with VACNTs grown in a 17 mm diameter circle. Growth conditions were 800 °C, 2666.5 Pa (20 Torr), 900 W applied microwave power, and 40 min growth. Conditions for the O_2 ash were an RF power of 200 W (30 kHz) at 66.67 Pa (0.5 Torr) for 60 s. Conditions for the CF_4 plasma were an RF power of 30 W (30 kHz) at 50 Pa (0.375 Torr) for 60 s. Details of the measurement are described in Ref. 3, and the optical setup is shown in Fig. 13. Measurement results of six samples are shown in Fig. 14 with uncertainties ($k = 2$) of 2%–3% (not shown).

APPENDIX D: FABRICATION STEPS

1. Planar cryogenic radiometer (PCR) (see Sec. IV)

- Select single-side polished (SSP) or double-side polished (DSP) Si wafer
- Grow thermal SiO_2 150 nm thick
- Backside: reactive ion etch (RIE) through SiO_2
- Photolithography, sputter deposit W 100 nm thick, lift-off
- Photolithography, sputter deposit Nb 100 nm thick, lift-off
- Photolithography, sputter deposit V 125 nm thick, lift-off
- PECVD of SiN_x 150 nm thick
- Photolithography, RIE through SiN_x
- Photolithography, sputter deposit AlO_x or AlN 10–20 nm thick and Fe 0.5–2 nm thick, lift-off
- Photolithography, RIE through SiO_2, DRIE through Si
- Grow VACNTs

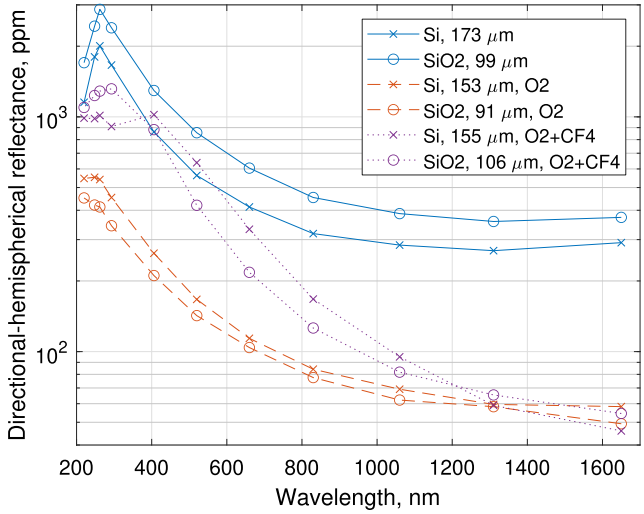

FIG. 14. Total (directional-hemispherical) reflectance in parts per million (ppm) of VACNT samples. Legend labels of "Si" or "SiO_2" specify the material directly under the catalyst support layer, the listed length is the VACNT height, "O_2" means the sample was exposed to an O_2 plasma, and "O_2 + CF_4" means the sample was exposed to an O_2 plasma followed by a CF_4 plasma. Uncertainties in reflectance (not shown) are 2%–3% ($k = 2$). See Ref. 3 for measurement details.

2. Compact spectral irradiance monitor (CSIM) (see Sec. V A)

- Select DSP Si wafer
- Grow thermal SiO_2 150 nm thick
- LPCVD of thermal SiN_x 2 μm thick
- Photolithography, RIE through SiN_x and SiO_2
- Backside: photolithography, RIE through SiN_x and SiO_2
- Photolithography, sputter deposit W 100 nm thick, lift-off
- Photolithography, sputter deposit AlO_x or AlN 10–20 nm thick and Fe 0.5–2 nm thick, lift-off
- Backside: photolithography, sputter deposit W 100 nm thick, lift-off
- Backside: DRIE through Si, stop at frontside SiO_2
- Grow VACNTs

Post-fabrication steps:

- Epoxy thermistor to bolometer
- Wirebond thermistor to W traces

3. Compact total irradiance monitor (CTIM) (see Sec. V B)

- Select thick DSP Si wafer (1 mm thick)
- Grow thermal SiO_2 1 μm thick
- Photolithography, sputter deposit W 100 nm thick, lift-off
- Backside: sputter deposit W 100 nm thick
- Backside: photolithography, RIE through W and SiO_2
- Photolithography, RIE through SiO_2
- Photolithography, sputter deposit W 100 nm thick, lift-off
- Photolithography, sputter deposit AlO_x or AlN 10–20 nm thick and Fe 0.5–2 nm thick, lift-off
- Photolithography, DRIE through Si
- Grow VACNTs

Post-fabrication steps:

- Epoxy four thermistors to bolometer
- Wirebond thermistors to W traces
- Epoxy dome to bolometer
- Attach bolometer to laser-cut polyimide legs

4. Pyranometer (see Sec. V C)

- Select DSP SOI wafer (layer thicknesses: device layer 50 μm, buried SiO_2 layer 500 nm, handle layer 475 μm)
- Grow thermal SiO_2 150 nm thick
- Photolithography, sputter deposit W 100 nm thick, lift-off
- Backside: photolithography, RIE through SiO_2
- Photolithography, sputter deposit AlO_x or AlN 10–20 nm thick and Fe 0.5–2 nm thick, lift-off
- Photolithography, RIE through SiO_2, DRIE through Si, RIE through buried SiO_2 layer
- Backside: DRIE through Si, stop at buried SiO_2 layer
- Grow VACNTs

5. Laser power metrology (see Sec. V D)

- Select DSP Si wafer
- Grow thermal SiO_2 150 nm thick
- LPCVD of thermal SiN_x 2 μm thick
- Backside: sputter deposit W 100 nm thick
- Photolithography, sputter deposit W 100 nm thick, lift-off
- Photolithography, sputter deposit W 100 nm thick, lift-off
- Backside: photolithography, RIE through W, SiN_x, and SiO_2
- Photolithography, sputter deposit AlO_x or AlN 10–20 nm thick and Fe 0.5–2 nm thick, lift-off
- Photolithography, RIE through SiN_x and SiO_2
- Photolithography, DRIE through Si
- Grow VACNTs

Post-fabrication steps:

- Epoxy two thermistors to bolometer
- Wirebond thermistors to W traces

6. Microbolometers (see Sec. V E)

- Select DSP Si wafer
- Grow thermal SiO_2 150 nm thick
- LPCVD of thermal SiN_x 2 μm thick
- Photolithography, RIE through SiN_x and SiO_2
- Backside: photolithography, RIE through SiN_x and SiO_2
- Photolithography, sputter deposit W 60 nm thick, lift-off
- Photolithography, sputter deposit VO_x 130 nm thick, lift-off
- Photolithography, sputter deposit W 120 nm thick, lift-off
- Photolithography, sputter deposit AlO_x or AlN 10–20 nm thick and Fe 0.5–2 nm thick, lift-off
- Backside: DRIE through Si, stop at frontside SiO_2
- Grow VACNTs

REFERENCES

[1] Z. Yang, L. Ci, J. A. Bur, S. Lin, and P. M. Ajayan, "Experimental observation of an extremely dark material made by a low-density nanotube array," Nano Lett. **8**, 446–451 (2008).
[2] C. J. Chunnilall, J. H. Lehman, E. Theocharous, and A. Sanders, "Infrared hemispherical reflectance of carbon nanotube mats and arrays in the 5–50 μm wavelength region," Carbon **50**, 5348–5350 (2012).
[3] C. S. Yung, N. A. Tomlin, K. Heuerman, M. W. Keller, M. G. White, M. Stephens, and J. H. Lehman, "Plasma modification of vertically aligned carbon nanotubes: Superhydrophobic surfaces with ultra-low reflectance," Carbon **127**, 195–201 (2018).
[4] C. S. Yung, N. A. Tomlin, J. Rutkowski, E. C. Richard, C. S. Yung, N. A. Tomlin, C. Straatsma, J. Rutkowski, E. C. Richard, D. M. Harber, J. H. Lehman, and M. S. Stephens, "BABAR: Black array of broadband absolute radiometers for far infrared sensing," Proc. SPIE **10980**, 109800F (2019).
[5] J. E. Martin, N. P. Fox, and P. J. Key, "A cryogenic radiometer for absolute radiometric measurements," Metrologia **21**, 147 (1985).
[6] A. A. Ayon, K.-S. Chen, K. A. Lohner, S. M. Spearing, H. H. Sawin, and M. A. Schmidt, "Deep reactive ion etching of silicon," in *Materials Research Society Proceedings, Symposium AA–Materials Science of Microelectromechanical Systems (MEMS)* (Cambridge University Press, 1999), Vol. 546, pp. 51–61.
[7] A. Gohier, C. P. Ewels, T. M. Minea, and M. A. Djouadi, "Carbon nanotube growth mechanism switches from tip- to base-growth with decreasing catalyst particle size," Carbon **46**, 1331–1338 (2008).
[8] M. Xu, D. N. Futaba, M. Yumura, and K. Hata, "Alignment control of carbon nanotube forest from random to nearly perfectly aligned by utilizing the crowding effect," ACS Nano **6**, 5837–5844 (2012).
[9] M. F. L. De Volder, S. J. Park, S. H. Tawfick, D. O. Vidaud, and A. J. Hart, "Fabrication and electrical integration of robust carbon nanotube micropillars by

self-directed elastocapillary densification," J. Micromech. Microeng. **21**, 045033 (2011).
[10]E. H. Cook and D. J. D. Carter, "MEMS process compatibility of multiwall carbon nanotubes," J. Vac. Sci. Technol., B **29**, 06FE04 (2011).
[11]N. A. Tomlin, A. E. Curtin, M. White, and J. H. Lehman, "Decrease in reflectance of vertically-aligned carbon nanotubes after oxygen plasma treatment," Carbon **74**, 329–332 (2014).
[12]M. E. Itkis, F. Borondics, A. Yu, and R. C. Haddon, "Bolometric infrared photoresponse of suspended single-walled carbon nanotube films," Science **312**, 413–416 (2006).
[13]A. Okamoto, I. Gunjishima, T. Inoue, M. Akoshima, H. Miyagawa, T. Nakano, T. Baba, M. Tanemura, and G. Oomi, "Thermal and electrical conduction properties of vertically aligned carbon nanotubes produced by water-assisted chemical vapor deposition," Carbon **49**, 294–298 (2011).
[14]N. A. Tomlin and J. H. Lehman, "Carbon nanotube electrical-substitution cryogenic radiometer: Initial results," Opt. Lett. **38**, 175–177 (2013).
[15]N. A. Tomlin, M. White, I. Vayshenker, S. I. Woods, and J. H. Lehman, "Planar electrical-substitution carbon nanotube cryogenic radiometer," Metrologia **52**, 376 (2015).
[16]K. D. Irwin, "An application of electrothermal feedback for high-resolution cryogenic particle-detection," Appl. Phys. Lett. **66**, 1998–2000 (1995).
[17]I. Ryger, D. Harber, M. Stephens, M. White, N. Tomlin, M. Spidell, P. Lobotka, and J. Lehman, "Low noise thermistor readout for wideband room temperature infrared detectors," in *2016 41st International Conference on Infrared, Millimeter, and Terahertz waves (IRMMW-THz)* (IEEE, 2016), pp. 1–2.
[18]I. Ryger, D. Harber, M. Stephens, M. White, N. Tomlin, M. Spidell, and J. Lehman, "Noise characteristics of thermistors: Measurement methods and results of selected devices," Rev. Sci. Instrum. **88**, 024707 (2017).
[19]M. White, "Characterisation of new planar cryogenic radiometric standards under development at NIST," in *Conference on Characterization and Radiometric Calibration for Remote Sensing (CALCON)*, 2016.
[20]J. Lehman, A. Steiger, N. Tomlin, M. White, M. Kehrt, I. Ryger, M. Stephens, C. Monte, I. Mueller, J. Hollandt, and M. Dowell, "Planar hyperblack absolute radiometer," Opt. Express **24**, 25911–25921 (2016).
[21]M. G. White, Z. E. Ruiz, C. S. Yung, I. Vayshenker, N. A. Tomlin, M. S. Stephens, and J. H. Lehman, "Cryogenic primary standard for optical fibre power measurement," Metrologia **55**, 706–715 (2018).
[22]S. I. Woods, J. Scherschligt, N. Tomlin, and J. Lehman, "Carbon nanotube radiometer for cryogenic calibrations," in *Conference on Characterization and Radiometric Calibration for Remote Sensing (CALCON)*, 2014.
[23]E. Richard, D. Harber, G. Drake, J. Rutkowsi, Z. Castleman, E. Richard, D. Harber, G. Drake, J. Rutkowsi, Z. Castleman, M. Smith, J. Sprunck, W. Zheng, P. Smith, M. Fisher, A. Sims, B. Cervelli, M. Fowle, M. Miller, M. Chambliss, T. Woods, P. Pilewskie, C. Yung, M. Stephens, N. Tomlin, M. White, and J. Lehman, "The compact spectral irradiance monitor flight demonstration mission," Proc. SPIE **11131**, 1113105 (2019).
[24]D. Harber, Z. Castleman, G. Drake, V. Dreser, N. Farber, D. Harber, Z. Castleman, G. Drake, S. V. Dreser, K. Heuerman, M. Miller, J. Rutkowski, A. Sims, C. Straatsma, I. Wanamaker, W. Zheng, E. Richard, P. Pilewskie, N. Tomlin, M. Stephens, C. Yung, M. White, and J. Lehman, "Compact total irradiance monitor flight demonstration," Proc. SPIE **11131**, 111310D (2019).
[25]M. Denoual, M. Pouliquen, G. Allegre, N. Tomlin, and J. Lehman, "Smart functions for carbon nanotube bolometer," in *2015 IEEE Sensors* (IEEE, Busan, 2015).
[26]M. S. Stephens, N. A. Tomlin, C. S. Yung, I. Ryger, M. White, J. H. Lehman, D. Harber, G. Kopp, K. Heuerman, J. Sprunck, Z. Castleman, G. Drake, and E. C. Richard, "From laboratory to CubeSat-room temperature absolute bolometers for laser power standards, solar spectral irradiance, and total solar irradiance," in *Conference on Characterization and Radiometric Calibration for Remote Sensing (CALCON)*, 2018.
[27]A. Vaskuri, M. S. Stephens, N. A. Tomlin, C. S. Yung, A. J. Walowitz, C. Straatsma, D. Harber, and J. H. Lehman, "Microfabricated bolometer based on a vertically aligned carbon nanotube absorber," Proc. SPIE **11269**, 112690L (2020).
[28]E. D. West, W. E. Case, A. L. Rasmussen, and B. Schmidt, "A reference calorimeter for laser energy measurements," J. Res. Natl. Bur. Stand., Sect. A **76A**, 13–26 (1972).
[29]G. L. Smith, K. J. Priestley, and N. G. Loeb, "Clouds and earth radiant energy system: From design to data," IEEE Trans. Geosci. Remote Sens. **52**, 1729–1738 (2014).
[30]S. Ilias, P. Topart, C. Larouche, P. Beaupré, D. Gay, C. Proulx, T. Pope, and C. Alain, "Deposition and characterization of gold black coatings for thermal infrared detectors," Proc. SPIE **7750**, 77501J (2010).
[31]F. Généreux, B. Tremblay, D. Gay, M. Briand, S. Deshaies, M. Poirier, J.-S. Caron, C. Alain, D. Béland, F. Provencal, D. Desbiens, J.-E. Paultre, and Y. Desroches, "Small uncooled bolometers with a broad spectral response," Proc. SPIE **10624**, 106241D (2018).
[32]C. S. Yung, N. A. Tomlin, and D. R. Schmidt, "Recessed carbon nanotube article and method for making same," U.S. Patent US20200003622A1 (2 January 2020 2019).
[33]A.-L. Biance, J. Gierak, É. Bourhis, A. Madouri, X. Lafosse, G. Patriarche, G. Oukhaled, C. Ulysse, J.-C. Galas, Y. Chen, and L. Auvray, "Focused ion beam sculpted membranes for nanoscience tooling," Microelectron. Eng. **83**, 1474–1477 (2006).
[34]A. Peltonen, H. Q. Nguyen, J. T. Muhonen, and J. P. Pekola, "Milling a silicon nitride membrane by focused ion beam," J. Vac. Sci. Technol., B **34**, 062201 (2016).
[35]G. Zhang, D. Mann, L. Zhang, A. Javey, Y. Li, E. Yenilmez, Q. Wang, J. P. McVittie, Y. Nishi, J. Gibbons, and H. Dai, "Ultra-high-yield growth of vertical single-walled carbon nanotubes: Hidden roles of hydrogen and oxygen," Proc. Natl. Acad. Sci. U. S. A. **102**, 16141–16145 (2005).
[36]Y. Chai, J. Gong, K. Zhang, P. C. H. Chan, and M. M. F. Yuen, "Low temperature transfer of aligned carbon nanotube films using liftoff technique," in *2007 Proceedings of the 57th Electronic Components and Technology Conference, ECTC '07* (IEEE, 2007), pp. 429–434.
[37]Y. Chai, J. Gong, K. Zhang, P. C. H. Chan, and M. M. F. Yuen, "Flexible transfer of aligned carbon nanotube films for integration at lower temperature," Nanotechnology **18**, 355709 (2007).
[38]M. Wang, T. T. Li, Y. G. Yao, H. F. Lu, Q. W. Q. Li, M. H. Chen, and Q. W. Q. Li, "Wafer-scale transfer of vertically aligned carbon nanotube arrays," J. Am. Chem. Soc. **136**, 18156–18162 (2014).
[39]A. Jungen, C. Stampfer, M. Tonteling, S. Schiesser, D. Sarangi, and C. Hierold, "Localized and CMOS compatible growth of carbon nanotubes on a 3 × 3 μm^2 microheater spot," in *The 13th International Conference on Solid-State Sensors, Actuators and Microsystems, 2005, Digest of Technical Papers, TRANSDUCERS '05* (IEEE, 2005), Vol. 1, pp. 93–96.
[40]Y. Zhou, J. Johnson, L. Wu, S. Maley, A. Ural, and H. Xie, "Design and fabrication of microheaters for localized carbon nanotube growth," in *2008 8th IEEE Conference on Nanotechnology* (IEEE, 2008), pp. 452–455.
[41]Y. Zhou, J. L. Johnson, A. Ural, and H. Xie, "Localized growth of carbon nanotubes on CMOS substrate at room temperature using maskless post-CMOS processing," IEEE Trans. Nanotechnol. **11**, 16–20 (2012).
[42]Y. van de Burgt, A. Champion, and Y. Bellouard, "*In-situ* localized carbon nanotube growth inside partially sealed enclosures," AIP Adv. **3**, 092119 (2013).
[43]Y. van de Burgt, W. van Loon, R. Mandamparambil, and Y. Bellouard, "Miniaturized reaction chamber for optimized laser-assisted carbon nanotube growth," J. Laser Micro/Nanoeng. **9**, 113–118 (2014).
[44]V. Svatoš, I. Gablech, B. R. Ilic, J. Pekárek, and P. Neužil, "*In situ* observation of carbon nanotube layer growth on microbolometers with substrates at ambient temperature," J. Appl. Phys. **123**, 114503 (2018).